

Barrier penetration effects in the triple-alpha reaction at low energies

Y. Suzuki^{1,2,*} and P. Descouvemont^{3,†}

¹*Department of Physics, Niigata University, Niigata 950-2181, Japan*

²*RIKEN Nishina Center, Wako 351-0198, Japan*

³*Physique Nucléaire Théorique et Physique Mathématique, C.P.229,
Université Libre de Bruxelles (ULB), B-1050 Brussels, Belgium*

We investigate the triple-alpha reaction at low energies, by assuming a direct process. The Coulomb potential of three α particles is examined carefully. The three-body continuum wave functions are generated by calculating an adiabatic potential barrier. We discuss the influence of the $\alpha\alpha$ potential, and compare our reaction rates with the literature. The reaction rate at $T = 0.01$ GK is about 10^3 times larger than that of NACRE.

PACS numbers: 26.20.Fj, 25.40.Lw, 21.45.-v

I. INTRODUCTION

The triple- α process plays an important role in stellar physics, since it triggers helium burning in stars. Owing to the absence of stable isotopes of mass 5 and 8, it represents the only way to synthesize ^{12}C in stars. At typical helium burning temperatures, the triple- α process is assumed to be sequential [1]. Two α particles are in equilibrium with the unstable ^8Be isotope, which then captures a third α . The second step, the $^8\text{Be}(\alpha, \gamma)^{12}\text{C}$ reaction, is strongly influenced by the ^{12}C 0_2^+ state ($E_x = 7.65$ MeV), located 0.29 MeV above the $\alpha+^8\text{Be}$ threshold. This resonance was predicted by Hoyle [1] and found experimentally later [2]. It is known, in the nuclear astrophysics community, as the Hoyle state. The properties (energy, alpha and gamma widths) of this resonance are well known experimentally.

The calculation of the triple- α reaction rate is, however, a subject of intense debate. First calculations [3–5] were based on the hypothesis of a sequential process, where the resonant nature of ^8Be and of the $^{12}\text{C}(0_2^+)$ resonance are accounted for by a Breit-Wigner (BW) approximation. For narrow resonances ($\Gamma_\alpha = 6$ eV in ^8Be , and $\Gamma_\alpha = 8.5$ eV in the Hoyle state), the BW formalism is expected to provide a fair approximation of the phase shifts and cross sections.

This simple approach was recently challenged by Ogata *et al.* [6] who use the continuum-discretized coupled-channels (CDCC) method [7]. In the CDCC theory, the ^8Be continuum is simulated by approximate, square-integrable wave functions. The CDCC method provides a consistent way to include the $\alpha + \alpha$ continuum in the calculation of the triple- α reaction rate. However, as the involved resonances are narrow, the BW approximation is expected to be reliable. CDCC results should therefore not be very different from results obtained previously in the literature. In fact, Ogata *et al.* found reaction rates much higher than those of NACRE (20 orders of mag-

nitude at low temperatures). At typical helium burning temperatures, the CDCC rates, when included in stellar models, are incompatible with observation [8].

The unexpectedly large CDCC results have triggered several theoretical studies, in different models. In particular the sequential picture was questioned by Garrido *et al.* [9] who suggest to extend the standard BW approximation to the three- α capture, which does not go through the ^8Be resonance. This simple direct model was then improved by Nguyen *et al.* [10] who use the hyperspherical formalism, associated with the R -matrix theory (HHR), to determine solutions of the $\alpha+\alpha+\alpha$ scattering problem. These approaches essentially confirm the NACRE reaction rate above $T \approx 0.1$ GK, where helium burning occurs. The large CDCC results cannot be explained. More recently, Ishikawa [11] investigated the triple- α problem in the Faddeev formalism. The results are essentially in agreement with NACRE, and much smaller than the recent three-body calculations.

Considering that the CDCC reaction rates above $T = 0.1$ GK are obviously inconsistent with observation, all other models agree in this temperature region, relevant for astrophysics. At lower temperatures, however, significant differences still exist between the various approaches. If the capture cross sections at these low energies are of minor importance in astrophysics, they raise interesting questions for nuclear physics aspects. The triple- α reaction rate offers a unique opportunity to investigate further three-body problems, in particular with three charged particles.

In this work, we address qualitatively the 3α system at low energies assuming a direct process, and we focus on general properties of the Coulomb interaction. A specific purpose is an attempt at understanding the reason for the differences of several orders of magnitude. In Sec. II we summarize the basic formulas to calculate the triple- α reaction rate according to the sequential and direct capture processes. We discuss in Sec. III general features of the Coulomb barrier for 3 α particles. The method used here is applicable for any Coulomb three-body problem. An adiabatic potential including the nuclear contribution is discussed in Sec. IV. The triple- α reaction rate is estimated assuming a simple 2^+ wave function of ^{12}C in

*Electronic address: suzuki@nt.sc.niigata-u.ac.jp

†Electronic address: pdesc@ulb.ac.be

Sec. V. Conclusion is drawn in Sec. VI. There are four appendices. We discuss totally symmetric hyperspherical harmonics (HH) in Appendix A, calculate the Coulomb matrix element in the hyperspherical coordinate in Appendix B, examine the convergence of the HH expansion in Appendix C, and analyze partial wave contents produced by symmetrization in Appendix D.

II. TRIPLE- α REACTION RATE

A. Sequential capture

Let us consider a process $2 + 3 + 4 \rightarrow 0 + 1$, where e.g., 2 stands for a nucleus with mass A_2 in the mass unit m . All masses of particles 2, 3 and 4 are assumed to be the same. Let $\langle 234 \rangle_{seq}$ denote the sequential reaction rate $R_{234}(E)$. In this approximation, the triple- α capture is assumed to proceed in two steps. According to Refs. [3, 4], the reaction rate is given by

$$\langle 234 \rangle_{seq} = 3 \left(\frac{8\pi\hbar}{\mu_{\alpha\alpha}^2} \right) \left(\frac{\mu_{\alpha\alpha}}{2\pi k_B T} \right)^{3/2} \times \int_0^\infty \frac{\sigma_{\alpha\alpha}(E)}{\Gamma_\alpha(^8\text{Be}, E)} \exp\left(-\frac{E}{k_B T}\right) \langle \sigma v \rangle^{\alpha^8\text{Be}} E dE, \quad (1)$$

where $\mu_{\alpha\alpha}$ is the reduced mass of the $\alpha + \alpha$ system, and E is the energy with respect to the $\alpha + \alpha$ threshold. The elastic cross section of $\alpha + \alpha$ scattering is given by a BW approximation, where the width of the ^8Be ground state is energy dependent.

The $\langle \sigma v \rangle^{\alpha^8\text{Be}}$ rate assumes that ^8Be has been formed at an energy E different from $E_{s\text{Be}}$, and that it is bound. This rate is given by

$$\langle \sigma v \rangle^{\alpha^8\text{Be}} = \frac{8\pi}{\mu_{\alpha^8\text{Be}}^2} \left(\frac{\mu_{\alpha^8\text{Be}}}{2\pi k_B T} \right)^{3/2} \times \int_0^\infty \sigma_{\alpha^8\text{Be}}(E'; E) \exp\left(-\frac{E'}{k_B T}\right) E' dE', \quad (2)$$

where $\mu_{\alpha^8\text{Be}}$ is the reduced mass of the $\alpha + ^8\text{Be}$ system, and E' is the energy with respect to its threshold (which varies with the formation energy E). Cross section $\sigma_{\alpha^8\text{Be}}(E'; E)$ corresponds to the $^8\text{Be}(\alpha, \gamma)^{12}\text{C}$ reaction, where E' is the $\alpha + ^8\text{Be}$ energy. This formalism has been used in the NACRE compilation for the calculation of the triple- α process [5].

B. Three-body capture

We present here a brief overview of the three-body capture. More detail can be found in Refs. [9, 12]. Let $\langle 234 \rangle^{3b}$ denote the reaction rate $R_{234}(E)$ averaged over the energy distribution

$$\langle 234 \rangle^{3b} = \int dE R_{234}(E) \frac{1}{2(k_B T)^3} E^2 \exp\left(-\frac{E}{k_B T}\right). \quad (3)$$

Similarly the inverse reaction process $0 + 1 \rightarrow 2 + 3 + 4$ has the thermonuclear reaction rate given by

$$\begin{aligned} \langle 01 \rangle &= \langle \sigma v \rangle_{01} \\ &= \int dE' \sigma_{01}(E') v' \frac{2}{\sqrt{\pi}(k_B T)^{3/2}} \sqrt{E'} \exp\left(-\frac{E'}{k_B T}\right) \\ &= \frac{2\sqrt{2}}{\sqrt{\pi}\mu_{01}(k_B T)^{3/2}} \int dE' \sigma_{01}(E') E' \exp\left(-\frac{E'}{k_B T}\right), \end{aligned} \quad (4)$$

where $E' = E - Q$ with the Q value for the reaction $0 + 1 \rightarrow 2 + 3 + 4$. In the case of the triple- α reaction, the Q value is $Q = -2.836$ MeV. We want to relate $R_{234}(E)$ to $\sigma_{01}(E')$.

The use of the detailed balance or reciprocity relation leads to

$$\begin{aligned} \frac{\langle 234 \rangle}{\langle 01 \rangle} &= \frac{g_0 g_1}{g_2 g_3 g_4} \left(\frac{A_0 A_1}{A_2 A_3 A_4} \right)^{3/2} \\ &\times \left(\frac{2\pi\hbar^2}{mk_B T} \right)^{3/2} \frac{1 + \Delta_{234}}{1 + \delta_{01}} \exp\left(-\frac{Q}{k_B T}\right). \end{aligned} \quad (5)$$

The validity of Eq. (5) relies on the time-reversal invariance of the Hamiltonian. It also implies that the first-order perturbation theory can be used.

In the case of $a + b + c \rightarrow A + \gamma$ process, σ_{01} denotes the photoabsorption cross section σ_γ with $E_\gamma = E - Q$ for $A + \gamma \rightarrow a + b + c$, and the above relation leads to the desired expression

$$\begin{aligned} R_{abc}(E) &= (1 + \Delta_{abc}) \frac{2g_A}{g_a g_b g_c} \frac{8\pi\hbar^3}{(\mu_{ab}\mu_{ab,c})^{3/2} c^2} \\ &\times \left(\frac{E_\gamma}{E} \right)^2 \sigma_\gamma(E_\gamma). \end{aligned} \quad (6)$$

See Refs. [9, 12] for the notations. If the photoabsorption occurs by an electric multipole $E\lambda$, its photoabsorption cross section can be expressed in terms of the strength function $S_{E\lambda}(E_\gamma)$ by

$$\sigma_\gamma(E_\gamma) = \frac{(2\pi)^3(\lambda+1)}{\lambda((2\lambda+1)!!)^2} \left(\frac{E_\gamma}{\hbar c} \right)^{2\lambda-1} S_{E\lambda}(E_\gamma), \quad (7)$$

where

$$\begin{aligned} S_{E\lambda}(E_\gamma) &= \frac{1}{2J_i + 1} \mathcal{S}_f |\langle \Psi_f | \mathcal{M}_{E\lambda} | \Psi_i \rangle|^2 \delta(E_f - E_i - E_\gamma). \end{aligned} \quad (8)$$

Here $\mathcal{M}_{E\lambda}$ is the $E\lambda$ operator, J_i is the angular momentum of the initial state and notation \mathcal{S}_f includes the integration over the final state energy E_f as well as the summation over the other quantum numbers that specify the final state.

III. TRIPLE- α COULOMB POTENTIAL

A. Hyperspherical coordinates

The Coulomb potential for a system including three charged particles is most transparently treated in the hyperspherical coordinates. Here we also express those operators that are relevant to the triple- α reaction in terms of the hyperspherical coordinates.

Let \mathbf{r}_i denote the coordinate of i th α particle. The intrinsic motion of 3 α system is described with two relative coordinates

$$\mathbf{x}_1 = \frac{1}{\sqrt{2}}(\mathbf{r}_1 - \mathbf{r}_2), \quad \mathbf{x}_2 = \sqrt{\frac{2}{3}}\left(\frac{\mathbf{r}_1 + \mathbf{r}_2}{2} - \mathbf{r}_3\right). \quad (9)$$

Other Jacobi coordinate sets $\mathbf{y}_1, \mathbf{y}_2$ and $\mathbf{z}_1, \mathbf{z}_2$ are respectively obtained by cyclic permutations (1, 2, 3) and (1, 3, 2) from $\mathbf{x}_1, \mathbf{x}_2$. The center of mass coordinate is denoted as $\mathbf{x}_3 = (\mathbf{r}_1 + \mathbf{r}_2 + \mathbf{r}_3)/3$.

The hyperradius ρ and five angular coordinates Ω_x are used in the HH method (see Ref. [13] for details). Four angle coordinates of Ω_x come from the angular coordinates $\hat{\mathbf{x}}_1 = \mathbf{x}_1/x_1$ and $\hat{\mathbf{x}}_2 = \mathbf{x}_2/x_2$, and the hyperangle α ($0 \leq \alpha \leq \pi/2$) is defined by

$$x_1 = \rho \cos \alpha, \quad x_2 = \rho \sin \alpha. \quad (10)$$

The hyperradius ρ is expressed in various ways:

$$\begin{aligned} \rho^2 &= x_1^2 + x_2^2 = \frac{1}{3} \sum_{j>i=1}^3 (\mathbf{r}_i - \mathbf{r}_j)^2 \\ &= \sum_{i=1}^3 (\mathbf{r}_i - \mathbf{x}_3)^2 \equiv 3\mathcal{M}_{00}. \end{aligned} \quad (11)$$

Here \mathcal{M}_{00} is the operator for the mean square radius. Note the difference in the definition of ρ in the literature. Our ρ is a half of the hyperradius of Ref. [10] and $1/\sqrt{2}$ of the hyperradius of Ref. [11]. Note also that the volume element for the six-dimensional integral is expressed as $d\mathbf{x}_1 d\mathbf{x}_2 = \rho^5 \cos^2 \alpha \sin^2 \alpha d\rho d\alpha d\hat{\mathbf{x}}_1 d\hat{\mathbf{x}}_2$.

The kinetic energy T of the 3 α system, with the center of mass kinetic energy being subtracted, is expressed as

$$\begin{aligned} T &= -\frac{\hbar^2}{2m_\alpha} \left(\frac{\partial^2}{\partial x_1^2} + \frac{\partial^2}{\partial x_2^2} \right) \\ &= -\frac{\hbar^2}{2m_\alpha} \left(\frac{\partial^2}{\partial \rho^2} + \frac{5}{\rho} \frac{\partial}{\partial \rho} - \frac{1}{\rho^2} \mathcal{K}^2 \right), \end{aligned} \quad (12)$$

where the hypermomentum operator \mathcal{K}^2 is given by

$$\mathcal{K}^2 = -\frac{\partial^2}{\partial \alpha^2} - 4 \cot 2\alpha \frac{\partial}{\partial \alpha} + \frac{1}{\cos^2 \alpha} \ell_1^2 + \frac{1}{\sin^2 \alpha} \ell_2^2. \quad (13)$$

Here ℓ_1 and ℓ_2 are the angular momenta corresponding to the coordinates \mathbf{x}_1 and \mathbf{x}_2 , respectively.

The $E2$ operator is expressed as

$$\begin{aligned} \mathcal{M}_{E2m} &= 2e \sum_{i=1}^3 \mathcal{Y}_{2m}(\mathbf{r}_i - \mathbf{x}_3) \\ &= 2e[\mathcal{Y}_{2m}(\mathbf{x}_1) + \mathcal{Y}_{2m}(\mathbf{x}_2)], \end{aligned} \quad (14)$$

with $\mathcal{Y}_{\ell m}(\mathbf{r}) = r^\ell Y_\ell^m(\hat{\mathbf{r}})$. Because ρ^2, \mathcal{K}^2 and \mathcal{M}_{E2m} are all symmetric operators, the \mathbf{x} coordinates can be replaced by the \mathbf{y} or \mathbf{z} coordinates, e.g., $\rho^2 = y_1^2 + y_2^2$ and $\mathcal{M}_{E2m} = 2e[\mathcal{Y}_{2m}(\mathbf{z}_1) + \mathcal{Y}_{2m}(\mathbf{z}_2)]$.

B. Triple- α Coulomb barrier

The Coulomb potential for 3 α particles can be treated in the HH method. Particularly we determine the Coulomb potential that gives the most enhanced triple- α reaction rate at low energies. In other words, the Coulomb potential should be as low as possible for 3 α particles.

The Coulomb potential for 3 α particles is expressed in hyperspherical coordinates as

$$V_C = \sum_{j>i=1}^3 \frac{4e^2}{|\mathbf{r}_i - \mathbf{r}_j|} = \frac{4e^2}{\rho} q(\Omega_x) \quad (15)$$

with a ‘charge factor’ operator

$$\begin{aligned} q(\Omega_x) &= \frac{1}{\sqrt{2}} \left\{ \frac{1}{\cos \alpha} + \frac{1}{\left| -\frac{1}{2} \cos \alpha \hat{\mathbf{x}}_1 + \frac{\sqrt{3}}{2} \sin \alpha \hat{\mathbf{x}}_2 \right|} \right. \\ &\quad \left. + \frac{1}{\left| -\frac{1}{2} \cos \alpha \hat{\mathbf{x}}_1 - \frac{\sqrt{3}}{2} \sin \alpha \hat{\mathbf{x}}_2 \right|} \right\}. \end{aligned} \quad (16)$$

As $q(\Omega_x)$ is symmetric with respect to the coordinate transformation, we may omit the suffix x of Ω_x .

Let us consider the eigenvalue problem

$$q(\Omega) F_q(\Omega) = q F_q(\Omega). \quad (17)$$

The eigenfunction $F_q(\Omega)$ must be symmetric with respect to the permutations of particles 1, 2, 3. The eigenvalue problem is solved using a complete set of the HH basis, $F_{KLM}^{\ell_1 \ell_2}(\Omega_x)$. Let $\{F_{KLM}^\gamma\}$ denote an orthonormal set of symmetric functions constructed from the HH basis, where γ is a suitable label to enumerate the symmetric functions (see Appendix A for details). A solution $F_q(\Omega)$ is expanded in the set $\{F_{KLM}^\gamma\}$. Unfortunately $q(\Omega)$ has non-vanishing matrix elements for $K \neq K'$, which is in fact the origin that makes a complete treatment of the Coulomb three-body problem extremely hard. A method of calculating the matrix element of $q(\Omega)$ is presented in Appendix B.

Figure 1 displays the spectrum of eigenvalues for $L = 0$ case as a function of K_{\max} , a maximum K value included in the diagonalization. Table I lists N (the basis dimension at K_{\max}), q_{\min} and q_{\max} , minimum and maximum

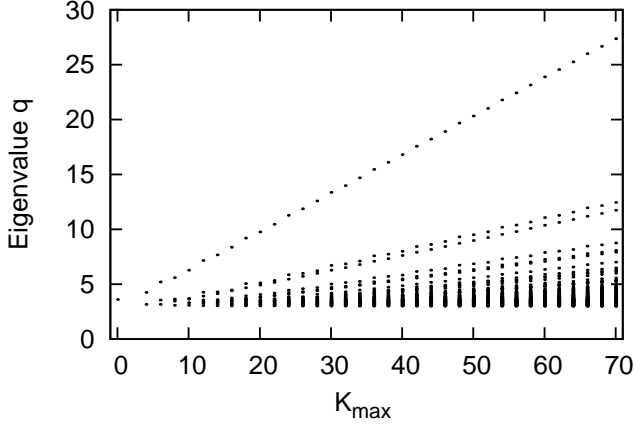


FIG. 1: Eigenvalues of q for 3α Coulomb potential as a function of K_{\max} .

TABLE I: Properties of the eigenvalues of 3α charge factor (16) as a function of K_{\max} .

K_{\max}	0	10	20	30	40	50	60	70
N	1	5	14	27	44	65	91	120
q_{\min}	3.601	3.076	3.021	3.012	3.006	3.005	3.003	3.002
q_{\max}	3.601	6.268	9.770	13.37	16.80	20.33	23.89	27.37
$\langle q \rangle$	3.601	4.000	4.140	4.214	4.216	4.236	4.247	4.248

eigenvalues of $q(\Omega)$ as well as $\langle q \rangle$, an average of the expectation values of $q(\Omega)$, i.e. the average of the eigenvalues

$$\langle q \rangle = \frac{1}{N} \sum_{\gamma=1}^N \langle F_{KLM}^\gamma | q(\Omega) | F_{KLM}^\gamma \rangle = \frac{1}{N} \text{Tr } q(\Omega). \quad (18)$$

The $\langle q \rangle$ value increases very slowly as K_{\max} increases. It starts from 3.601 at $K_{\max} = 0$ and reaches about 4.25 at $K_{\max} = 70$. It is remarkable that q_{\min} approaches 3 and does not become smaller than 3. On the other hand, q_{\max} increases monotonically as a function of K_{\max} .

As seen above, the spectrum of eigenvalues varies as a function of K_{\max} . This is a consequence of possible arrangements that 3α particles can take for a given K_{\max} . With increasing K_{\max} not only q_{\min} approaches 3 but also an increasing number of eigenfunctions have q values very close to 3. Classically we expect $q = 3$ assuming a regular triangle configuration of 3α particles because then ρ is equal to its side length as indicated by Eq. (11) and its Coulomb potential, $3 \times 4e^2/\rho$, gives $q = 3$. The value of q_{\max} is, however, isolated from the other eigenvalues. It approximately follows a straight line, $q_{\max} \approx 0.35K_{\max} + 2.8$ for $K_{\max} \geq 4$.

The Coulomb potential is now represented as $V_C(\rho) = 4e^2q/\rho$ with use of the eigenvalue q . In the representation that diagonalizes $q(\Omega)$ the Coulomb potential has no

coupling at all. The value of q_{\min} is of particular interest in the low energy triple- α reaction because it leads to a minimum Coulomb barrier.

IV. ADIABATIC POTENTIAL BARRIER

The initial state Ψ_i of Eq. (8) is confined in a small region around the center of mass of the 3α particles. However, the final continuum state at very low energy has to penetrate through a thick barrier to reach the asymptotic region where its normalization is preset. It is crucially important to evaluate properly the barrier for 3α particles in order to obtain the photoabsorption cross section at low energies. The barrier may be calculated in the adiabatic hyperspherical expansion method [14, 15], where the potential energy acting among α particles is diagonalized on the hypersphere with a radius ρ . Repeating this calculation for a number of ρ values, one obtains an adiabatic potential. This may be akin in spirit to what is done for the Coulomb potential in Sect. IIIB. Contrary to the Coulomb case where the ρ -dependence is trivially known, one has to repeat the diagonalization at each ρ .

Since the HH expansion is known to converge slowly as discussed in Appendix C, one may take other trial function, $\Psi = \sum_{\xi} C_{\xi} \Phi(\xi)$, where $\Phi(\xi)$ is a basis function depending on some parameters ξ . The barrier at ρ can be obtained by minimizing the energy $\langle \Psi | H | \Psi \rangle / \langle \Psi | \Psi \rangle$ with respect to C_{ξ} under the constraint $\langle \rho^2 \rangle = \rho^2$. Here we adopt a product of Gauss wave packets specified by two ‘generator coordinates’ \mathbf{s}_1 and \mathbf{s}_2

$$\Phi(\mathbf{s}_1, \mathbf{s}_2, \mathbf{x}) = \left(\frac{\beta}{\pi} \right)^{3/4} \exp(-\frac{1}{2}\beta(\mathbf{x}_1 - \mathbf{s}_1)^2) \times \left(\frac{\beta}{\pi} \right)^{3/4} \exp(-\frac{1}{2}\beta(\mathbf{x}_2 - \mathbf{s}_2)^2). \quad (19)$$

The value of β is related to the mean square radius of α particle. It is chosen as $\beta = 4 \times 0.52 \text{ fm}^{-2}$ based on the $(0s)^4$ harmonic-oscillator shell-model wave function for α particle [16]. We symmetrize the wave function $\Phi(\mathbf{s}_1, \mathbf{s}_2, \mathbf{x})$ to calculate the potential energy matrix element. The expectation value of the potential energy, $V(\mathbf{s}_1, \mathbf{s}_2)$, is an estimate of the barrier corresponding to the geometric arrangement specified by \mathbf{s}_1 and \mathbf{s}_2 .

In this study we do not minimize the energy but approximately obtain the barrier by averaging $V(\mathbf{s}_1, \mathbf{s}_2)$ over \mathbf{s}_1 and \mathbf{s}_2 with the constraint of $s_1^2 + s_2^2 = s^2 = \rho^2$:

$$V(\rho) = \frac{1}{\rho^5} \int d\mathbf{s}_1 \int d\mathbf{s}_2 V(\mathbf{s}_1, \mathbf{s}_2) w(\Omega_s) \delta(s - \rho) \quad (20)$$

with a weight function $w(\Omega_s)$ that satisfies the normalization

$$\int d\Omega_s w(\Omega_s) = 1. \quad (21)$$

The $1/\rho^5$ factor of Eq. (20) arises because of the property $\int d\mathbf{s}_1 \int d\mathbf{s}_2 w(\Omega_s) \delta(s-\rho) = \int ds s^5 \int d\Omega_s w(\Omega_s) \delta(s-\rho) = \rho^5$. Any $w(\Omega_s)$ that meets Eq. (21) is expressed as

$$w(\Omega_s) = \sum_{K\ell} C_{K\ell} F_{K00}^{\ell\ell}(\Omega_s) \quad (22)$$

with the constraint $C_{00} = F_{000}^{00}(\Omega_s) = \pi^{-3/2}$.

We choose $C_{K\ell} = C_{00} \delta_{K,0} \delta_{\ell,0}$ to project out only $K = 0$ barrier, which leads to the adiabatic potential

$$V(\rho) = \frac{1}{\pi^3 \rho^5} \int d\mathbf{s}_1 \int d\mathbf{s}_2 V(\mathbf{s}_1, \mathbf{s}_2) \delta(s - \rho). \quad (23)$$

Note that the adiabatic potential of this choice approaches $4e^2 \times 3.601/\rho$ for large ρ , where only the Coulomb potential contributes to the barrier. The value of 3.601 is the eigenvalue of q at $K = 0$. We modify the Coulomb contribution to its minimum at large ρ in calculating the photoabsorption cross section.

The kinetic energy (12) contains the centrifugal potential. Its form is apparent for $\psi = \rho^{5/2} \Psi_f$ [13], and its contribution to the adiabatic potential reads

$$\begin{aligned} V_{CF}(\rho) &= \frac{\hbar^2}{2m_\alpha \rho^2} \int d\Omega_s [\mathcal{K}^2(\Omega_s) + \frac{15}{4}] w(\Omega_s) \\ &= \frac{\hbar^2}{2m_\alpha \rho^2} \frac{15}{4}. \end{aligned} \quad (24)$$

Thus the centrifugal potential also becomes a minimum. As the result our adiabatic potential barrier turns out to be lowest regarding the Coulomb and centrifugal potentials. In this case the centrifugal potential becomes less than 1% of the Coulomb potential only when ρ is larger than 115 fm.

Panels (a) and (b) of Fig. 2 display the adiabatic potentials calculated with Ali-Bodmer A' (AB(A')) and Ali-Bodmer D (AB(D)) $\alpha\alpha$ potentials [14, 17], respectively. The mass of α particle is $\hbar^2/m_\alpha = 10.5254 \text{ MeV fm}^2$, and the charge constant is $e^2 = 1.43996 \text{ MeV fm}$. The contributions from the $\alpha\alpha$ nuclear and Coulomb potentials as well as the three-body force are also shown. All of the potential parameters are the same as those of Ref. [11]. The AB(A') potential is used also in Ref. [10], but its three-body force is different from the present one. The barrier peak is 1.1 MeV at $\rho = 12.4 \text{ fm}$ for AB(A') and 1.5 MeV at $\rho = 9.3 \text{ fm}$ for AB(D), respectively. Because the AB(D) potential contains stronger repulsion at short distances, the minimum of the adiabatic potential is rather shallow and located at distance larger than that of AB(A') potential. The adiabatic potential of AB(A') is deep enough to produce a resonance. The energy and width of the resonance are 0.702 MeV and 6 keV, so that its energy is too high and its width is too wide to be compared to those (0.379 MeV, 8.5 eV) of the Hoyle state. Note that each piece of the Hamiltonian contributes differently in its distance of reach. The $\alpha\alpha$ nuclear contribution decreases rather slowly as a function of ρ . In the case of AB(D) potential, it becomes 1% of

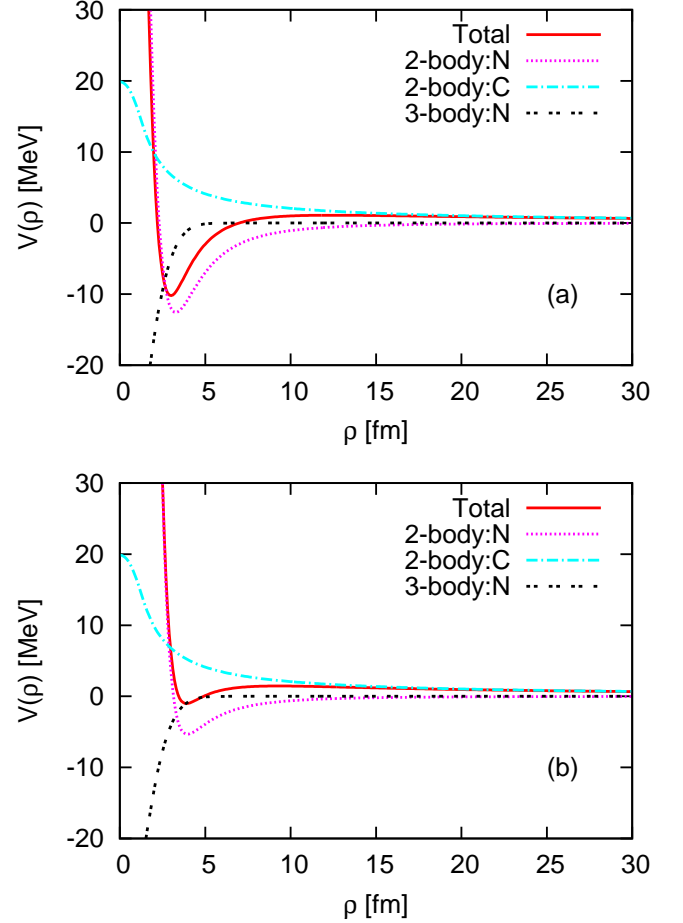


FIG. 2: (Color online) The adiabatic potential for AB(A') (a) and AB(D) (b) potentials including 3-body potential. The potential parameters are taken from Ref. [11].

the Coulomb contribution only when ρ is larger than 50 fm.

To see the effect of the symmetrization, we also calculate the adiabatic potential using the wave function (19) itself. Most noteworthy is that the Coulomb barrier evaluated by ignoring the boson symmetry is smaller by about 7% for any ρ than the one calculated with the symmetrized wave function. For example, the non-symmetrized Coulomb barrier approaches $4e^2 \times 3.35/\rho$ for large ρ instead of $4e^2 \times 3.60/\rho$.

V. CALCULATION OF TRIPLE- α REACTION RATES AT LOW ENERGIES

A. Wave functions

The triple- α reaction rate (6) can be calculated from the photoabsorption cross section $\sigma_\gamma(E_\gamma)$ of Eq. (7) for

E2. The result is

$$R_{\alpha\alpha\alpha}(E) = 1440\sqrt{3}\pi\frac{\hbar^3}{m_\alpha^3c^2}\left(\frac{E_\gamma}{E}\right)^2\sigma_\gamma(E_\gamma), \quad (25)$$

where $E_\gamma = E + 2.836$ in MeV.

To obtain σ_γ , we take a simple model for the initial and final states. The 2^+ initial bound state is assumed to be

$$\Psi_{2M} = \mathcal{N} \exp(-\frac{1}{2}a\rho^2)(\mathcal{Y}_{2M}(\mathbf{x}_1) + \mathcal{Y}_{2M}(\mathbf{x}_2)), \quad (26)$$

where $\mathcal{N} = \sqrt{8a^5/15\pi^2}$ is the normalization constant. This wave function satisfies the boson symmetry. The parameter a is related to the root-mean-square (rms) radius of the 2^+ state of ^{12}C . The mean square radius $\langle\rho^2\rangle$ of the 3α system is related to that of ^{12}C , $\langle r_C^2\rangle$, by the following relation

$$\langle r_C^2\rangle = \langle r_\alpha^2\rangle + \langle \mathcal{M}_{00}\rangle = \langle r_\alpha^2\rangle + \frac{1}{3}\langle\rho^2\rangle, \quad (27)$$

where $\langle r_\alpha^2\rangle$ is the mean square radius of α particle. The value of $\langle\rho^2\rangle$ calculated with Eq. (26) is $\langle\rho^2\rangle = 5/a$. We adopt $\sqrt{\langle r_C^2\rangle} \approx 2.45$ fm based on theoretical calculations [18], which leads to a choice of $a = 0.43$ fm $^{-2}$.

To check the reliability of the 2^+ wave function (26) for evaluating the $E2$ matrix element, we determine the quadrupole moment of the 2^+ state. The intrinsic quadrupole moment, $Q_0 = \sqrt{16\pi/5}\langle\Psi_{22}|\mathcal{M}_{E20}|\Psi_{22}\rangle$, is obtained as $Q_0 = -(4/a)e = -9.3 e\text{fm}^2$, which is compared to the experimental value, $-22 \pm 10 e\text{fm}^2$ [19]. Our model wave function appears to give slightly small quadrupole deformation.

The final continuum state Ψ_f regular at the origin is obtained as follows. In a single-channel approximation with the adiabatic potential (20), the equation of motion for $\psi(E, \rho) = \rho^{5/2}\Psi_f$ with energy E is derived using Eq. (12) as

$$\left(\frac{d^2}{d\rho^2} - \frac{\Lambda(\Lambda+1)}{\rho^2} + k^2 - \frac{2m_\alpha}{\hbar^2}V(\rho)\right)\psi(E, \rho) = 0, \quad (28)$$

where $k^2 = 2m_\alpha E/\hbar^2$ and $\Lambda = 3/2$. To obtain a solution $\psi(E, \rho)$, we note that $V(\rho)$ approaches $Z_{\text{eff}}e^2/\rho$ ($Z_{\text{eff}} = 12$) for large ρ . Therefore the solution of Eq. (28) at large ρ can be expressed as a combination of regular and irregular Coulomb wave functions $F_\Lambda(\eta, \rho)$ and $G_\Lambda(\eta, \rho)$, where $\eta = m_\alpha Z_{\text{eff}}e^2/\hbar^2k$. Note, however, that $\psi(E, \rho)$ in the asymptotic region is subject to the $\delta(E - E')$ normalization of Ψ_f . That is, $\psi(E, \rho)$ satisfies

$$\psi(E, \rho) \rightarrow \sqrt{\frac{2m_\alpha}{\pi^4\hbar^2k}}[\cos\delta F_\Lambda(\eta, \rho) + \sin\delta G_\Lambda(\eta, \rho)] \quad (29)$$

for large ρ . Here δ is the three-body phase shift.

B. $E2$ strength function and reaction rate

The $E2$ strength function (8) for the transition from the 2^+ state to the continuum is given by

$$S_{E2}(E_\gamma) = \frac{5\pi^2 e^2}{96} a^5 [I_{i\rightarrow f}(E)]^2 \quad (30)$$

with the radial integral between the initial and final states

$$I_{i\rightarrow f}(E) = \int_0^\infty d\rho \rho^{13/2} \psi(E, \rho) \exp(-\frac{1}{2}a\rho^2). \quad (31)$$

The integral $I_{i\rightarrow f}(E)$ plays a decisive role to determine the reaction rate. The amplitude of $\psi(E, \rho)$ in the region that contributes to the integral is determined by the potential $V(\rho)$ from the asymptotic region down to the internal region as the normalization of $\psi(E, \rho)$ is fixed asymptotically. The lower the potential barrier, the larger the reaction rate.

Panels (a) and (b) of Fig. 3 display the integrand of $I_{i\rightarrow f}(E)$ for AB(A') and AB(D) potentials, respectively.

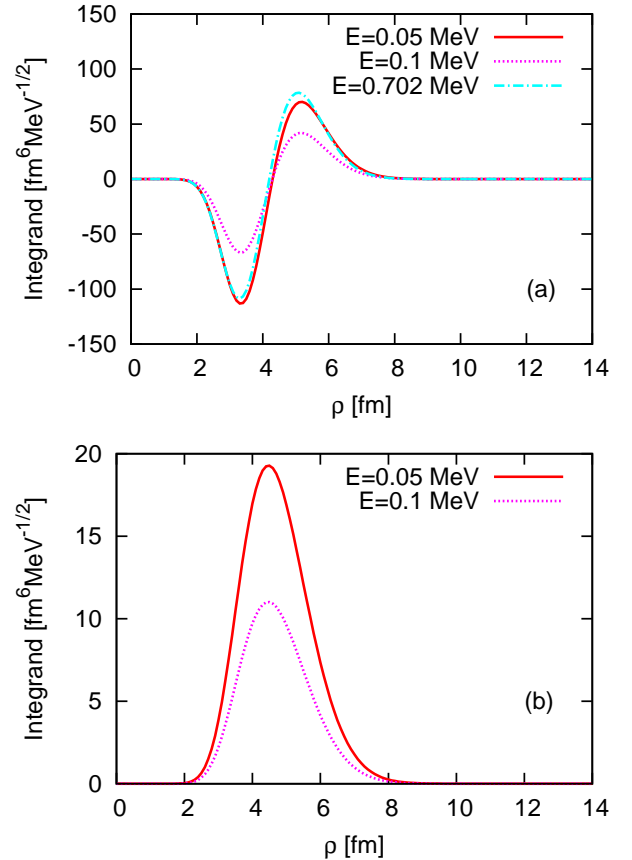


FIG. 3: (Color online) The integrand of $I_{i\rightarrow f}(E)$ for AB(A') (a) and AB(D) (b) potentials as a function of ρ . Plotted curves are magnified by $3 \cdot 10^{19}$ for $E = 0.05$ MeV and by $3 \cdot 10^{12}$ for $E = 0.1$ MeV, respectively. No multiplication is made for $E = 0.702$ MeV curve.

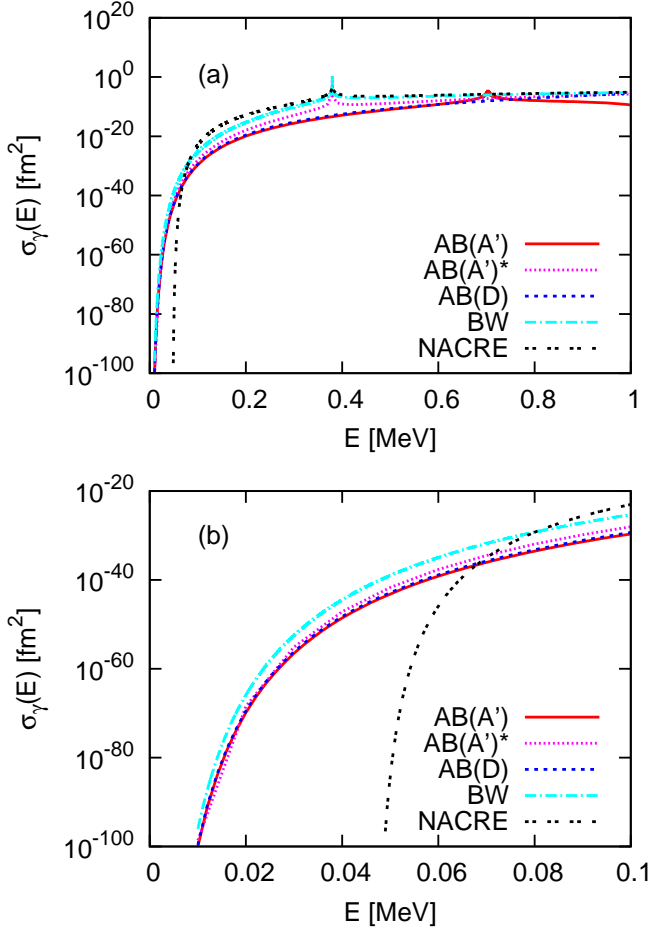


FIG. 4: (Color online) Photoabsorption cross section of the 2^+ state of ^{12}C into 3α 0^+ continuum state with the 3α energy E . Panel (b) enlarges panel (a) at low energies. The photoabsorption cross sections calculated according to NACRE model [5] and BW formula (Eq. (4) of Ref. [9]) for the direct process are also shown.

The shape of the integrand looks very similar in each case. It is remarkable that the integrand of $\text{AB}(A')$ has a node that is almost energy-independent, while the one of $\text{AB}(D)$ has no such node. The reason is that the adiabatic potential calculated with $\text{AB}(A')$ is deep enough to accommodate a 0^+ bound state, so that the continuum wave function has to be orthogonal to that bound state. Since the $\text{AB}(D)$ potential supports no bound state, however, the continuum wave function in that adiabatic potential can reach the inner region without the orthogonality constraint. Moreover, the magnitude of the integrand is quite different. With the $\text{AB}(A')$ interaction, we expect a strong cancellation for $I_{i \rightarrow f}(E)$, whereas no such cancellation occurs in $\text{AB}(D)$. The magnitude of the integrand of $\text{AB}(A')$ is much larger than that of $\text{AB}(D)$.

Figure 4 displays the photoabsorption cross section $\sigma_\gamma(E)$ calculated with the $\text{AB}(A')$ and $\text{AB}(D)$ potentials together with NACRE and BW cross sections. We also

show $\text{AB}(A')^*$ calculation that uses the $\text{AB}(A')$ potential with the strength of the three-body force being adjusted to reproduce the Hoyle resonance energy. The calculated resonance width is, however, too small to be compared to experiment. Table II compares the low-energy σ_γ values calculated by the several models in ratio to NACRE cross sections [9]. The present result is between BW and Faddeev. In the BW model, the low-energy σ_γ is controlled by the width $\Gamma_{3\alpha}$, which is not yet determined experimentally and is simply assumed to be equal to the total width Γ of the Hoyle state. However, since the Hoyle state decays predominantly via the $\alpha + {}^8\text{Be}(0^+)$ channel, $\Gamma_{3\alpha}$ is probably considerably smaller than Γ [20]. Thus the BW value may be considered as the upper limit of the direct process at very low energies. As shown in the table, all of σ_γ values calculated by different models are very much enhanced compared to NACRE at 0.05 MeV, but there is a big difference among them: The HHR result is much larger than the BW value, while the Faddeev gives smaller value. At $E = 0.1$ MeV the difference among the models becomes smaller.

Figure 5 compares the energy averaged triple- α reaction rate with NACRE. Both $\text{AB}(A')$ and $\text{AB}(A')^*$ give almost the same reaction rate. Because the properties of the Hoyle resonance are not reproduced in the present calculation, the reaction rate above $T = 0.1$ GK is much smaller than the NACRE rate. Table II compares our reaction rates at 0.01 and 0.03 GK with those obtained by BW, HHR, Faddeev, and CDCC calculations. The huge enhancement of CDCC calculation is not supported by any other calculations. However, the enhancement compared to NACRE is still at variance depending on the model. We see that both present and Faddeev calculations give rather close results at the two temperatures. Compared to these, HHR rate is larger by 10^{15} and BW rate is larger by 10^4 at 0.01 GK. Though the difference tends to decrease at 0.03 GK, there is still a difference by about 10^7 at maximum.

C. Symmetrization effects

We examine the extent to which the neglect of symmetrization changes the reaction rate. We use the $\alpha\alpha$ potential of Ref. [6] and calculate the adiabatic potential using the wave function of Eq. (19) itself (non-symmetrized version) and its symmetrized wave function (symmetrized version). Figure 6 compares the photoabsorption cross sections obtained with the adiabatic potential of the non-symmetrized version with the one of the symmetrized version. The non-symmetrized cross section is more than 10^6 times larger than the symmetrized one at, e.g., 0.01 MeV, but the enhancement of the energy-averaged reaction rate $\langle R_{\alpha\alpha\alpha} \rangle$ is more moderate as shown in Fig. 7. At very low temperature where the non-resonant contribution is expected to be important, the enhancement is on the order of 10^3 at $T = 0.01$ GK. A part of the reason for the huge enhancement reported in

TABLE II: Comparison of the photoabsorption cross section σ_γ and the Maxwell-Boltzmann energy-averaged triple-alpha reaction rate $N_A^2 \langle R_{\alpha\alpha\alpha} \rangle$. AB(A') potential is used except for BW and CDCC. Values in parentheses are obtained with AB(D) potential, while those with * are obtained with AB(A')* potential. The cross sections are given in ratio to NACRE [5], which is 1.6×10^{-84} at $E = 0.05$ and $9.7 \times 10^{-24} \text{ fm}^2$ at $E = 0.1 \text{ MeV}$, respectively. The reaction rate is also given in ratio to NACRE, which is 2.9×10^{-71} at $T = 0.01$ and $1.5 \times 10^{-47} \text{ cm}^6 \text{ s}^{-1} \text{ mol}^{-2}$ at $T = 0.03 \text{ GK}$, respectively.

σ_γ					
$E(\text{MeV})$	Present	BW [9]	HHR [10]	Faddeev [11]	
0.05	$4 \cdot 10^{40} (9 \cdot 10^{40})$ $1 \cdot 10^{42*}$	$6 \cdot 10^{44}$	$2 \cdot 10^{52}$	$1 \cdot 10^{38} (8 \cdot 10^{37})$	
0.1	$2 \cdot 10^{-7} (5 \cdot 10^{-7})$ $1 \cdot 10^{-5*}$	$5 \cdot 10^{-3}$	$4 \cdot 10^{-3}$	$3 \cdot 10^{-8} (3 \cdot 10^{-8})$	
$N_A^2 \langle R_{\alpha\alpha\alpha} \rangle$					
$T(\text{GK})$	Present	BW [9]	HHR [10]	Faddeev [11]	CDCC [6]
0.01	$2 \cdot 10^3 (4 \cdot 10^3)$ $2 \cdot 10^{3*}$	$3 \cdot 10^7$	$3 \cdot 10^{18}$	$1 \cdot 10^1 (5 \cdot 10^0)$	$4 \cdot 10^{26}$
0.03	$2 \cdot 10^0 (5 \cdot 10^0)$ $2 \cdot 10^0*$	$5 \cdot 10^4$	$1 \cdot 10^7$	$2 \cdot 10^0 (9 \cdot 10^{-1})$	$2 \cdot 10^{18}$

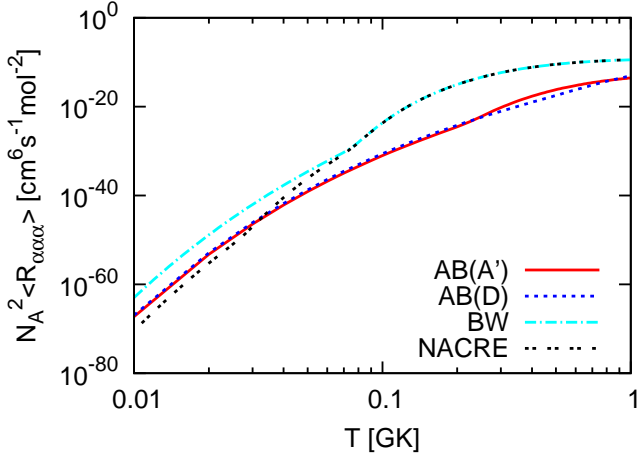


FIG. 5: (Color online) The same as Fig. 4 but for the Maxwell-Boltzmann energy-averaged triple- α reaction rate as a function of temperature T .

Ref. [6] is due to this neglect of the symmetrization, but its effect is not large enough to account for such huge enhancement as 10^{26} at 0.01 GK.

D. Discussion of the literature

In the following we attempt at understanding possible reasons for the large photoabsorption cross sections of CDCC and HHR. The calculations of Refs. [6, 11] are performed in the Jacobi coordinates, $\mathbf{r} = \sqrt{2}\mathbf{x}_1$ and $\mathbf{R} = \sqrt{3/2}\mathbf{x}_2$. With these coordinates the Coulomb po-

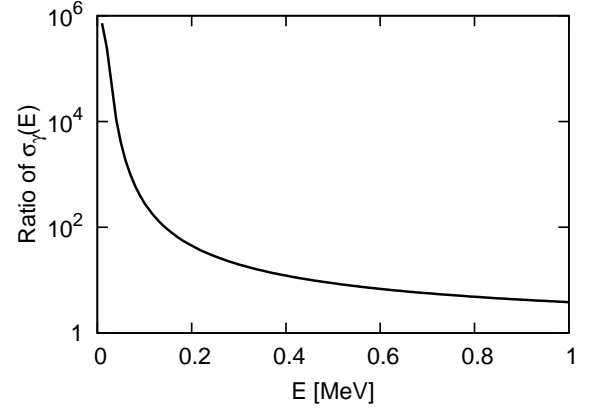


FIG. 6: Ratio of the photoabsorption cross sections calculated with the non-symmetrized and symmetrized wave functions as a function of the 3α energy E . The adiabatic potential is obtained with the $\alpha\alpha$ potential of Ref. [6].

tential (15) is expanded in multipoles as

$$V_C = \frac{4e^2}{r} + \frac{8e^2}{R_{>}} \sum_{\ell=\text{even}} \left(\frac{R_{<}}{R_{>}} \right)^\ell P_\ell(\hat{\mathbf{r}} \cdot \hat{\mathbf{R}}), \quad (32)$$

where $R_{>}(R_{<})$ denotes the larger (smaller) between R and $r/2$, and P_ℓ is the Legendre polynomial of degree ℓ . Thus the coupling between \mathbf{r} and \mathbf{R} is always present everywhere, and it is crucial to take care of such couplings in the calculation. The 3α continuum wave function may be written in the spirit of CDCC as

$$\Psi \sim \sum_i \frac{u_i(r)}{r} \frac{\chi_i(R)}{R} [Y_{\ell_i}(\hat{\mathbf{r}}) Y_{\ell_i}(\hat{\mathbf{R}})]_{00} + \Psi_{\text{dc}}, \quad (33)$$

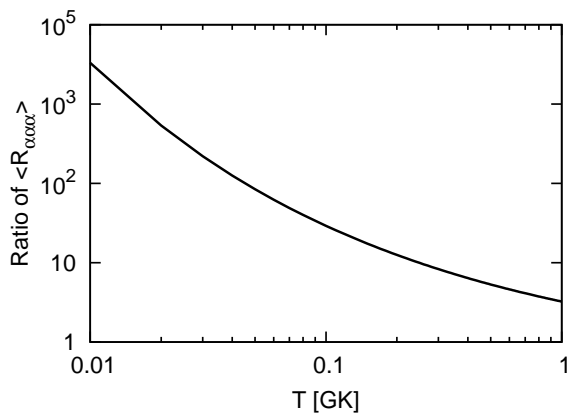


FIG. 7: The same as Fig. 6 but for the ratio of the Maxwell-Boltzmann energy-averaged triple- α reaction rate as a function of temperature T .

where $u_i(r)Y_{\ell_i}(\hat{\mathbf{r}})$ is the $\alpha\alpha$ continuum-discretized state of i th bin and Ψ_{dc} , vanishing asymptotically, stands for square-integrable distorted components other than the first term. Neither high-partial waves nor Ψ_{dc} is included in Ref. [6].

The contribution of the Coulomb potential to the coupling potential reads

$$V_{ij}^C(R) = \frac{8e^2}{R} \sum_{\ell=\text{even}} C_{ij}^{\ell} \left\{ \int_0^{2R} dr u_i^*(r) u_j(r) \left(\frac{r}{2R}\right)^{\ell} + \int_{2R}^{\infty} dr u_i^*(r) u_j(r) \left(\frac{2R}{r}\right)^{\ell+1} \right\}, \quad (34)$$

where C_{ij}^{ℓ} is a matrix element of type (B5). The coupling potential in general never vanishes even for large R , but if only S wave is included, no coupling arises at large R . The truncation to S wave only will thus lead to enhancing the reaction rate to some extent. At least D wave has to be included.

More important is the role of Ψ_{dc} . There are a number of cases that demonstrate the importance of Ψ_{dc} to obtain converged solutions for scattering and radiative capture reactions (see, e.g., Refs. [21–24]). The form of Ψ_{dc} depends on the problem concerned. In the present case a primary concern is to take proper account of the Coulomb potential of 3α particles. Most of $u_i(r)$'s included in the CDCC calculation [6] are spread to large distances, so that the first term of Eq. (33) alone may not be flexible enough to represent the damping of the amplitude of Ψ in the region where the photoabsorption occurs. If this is the case, an explicit inclusion of some distorted configurations is needed to make Ψ realistic, which would lead to a smaller reaction rate.

In the HHR calculation [10] the hyperspherical coordinate is used instead of \mathbf{r} and \mathbf{R} . Choosing the R -matrix radius to be $\rho = 25$ fm, the 3α wave function inside the region is expanded as a superposition of the HH func-

tions with $K_{\text{max}} \approx 26$, and then it is propagated to the asymptotic region. The $E2$ strength function of HHR is much larger than the present one at $E \leq 0.05$ MeV. This indicates that the amplitude of the HHR continuum state is very much enhanced at the low energies. One possible reason for this may be in the tail behavior of the Coulomb potential. In the HHR the Coulomb coupling is taken into account up to $\rho = 400$ fm keeping $K_{\text{max}} \approx 26$ and, after that the off-diagonal coupling is screened up to 1500 fm. This procedure together with the R -matrix propagation of $K_{\text{max}} \approx 26$ truncation might lead to the tail behavior that is different from ours. As shown in Table III and Fig. 8 of Appendix C, the convergence of the HH expansion becomes slower as the size of 3α system becomes larger. This suggests that the K truncation made in the innermost region may result in preventing the continuum wave function from spreading to many more K components during the process of R -matrix propagation.

VI. CONCLUSION

We address the triple-alpha reaction at very low energies to obtain its reaction rate below 0.1 GK. On the basis of the direct capture process of three α particles, we discuss the potential barrier through which 3α particles penetrate and fuse to make the radiative transition to the 2^+ state of ^{12}C . The general properties of the 3α Coulomb potential that dominates the barrier at large distances are carefully examined in hyperspherical coordinates and the minimum Coulomb barrier is established. Since the hyperspherical harmonics (HH) expansion is slow as the size of 3α system expands, the adiabatic potential barrier as a function of the hyperradius is estimated by averaging the potential energy expectation values of various geometric configurations specified by Gauss wave packets.

Our results on the triple-alpha rate do not support the large continuum-discretized coupled-channels (CDCC) values at 0.01 GK, but fall between those of the Breit-Wigner model and the Faddeev method. We attempt at understanding possible mechanism of how the large rate is obtained in the CDCC and HH basis R -matrix calculations. Though it is simply assumed as the average potential energy in the present study, the adiabatic potential barrier should in principle be obtained by taking into account the coupling of various configurations. A study along this extension will be interesting. A final goal will be a microscopic study of the triple-alpha reaction process.

Acknowledgments

One of the authors (Y.S.) thanks E. Garrido for several illuminating correspondences as well as for his codes of the Breit-Wigner cross sections. He is indebted to

D. Baye for useful discussions and the support for his stay at ULB, June 2013, where a part of this work was performed. The work of Y.S. is supported in part by Grant-in-Aid for Scientific Research (No. 24540261) of the Japan Society for the Promotion of Science. P.D. is Directeur de Recherches F.R.S.-FNRS.

Appendix A: Symmetric hyperspherical harmonics

An orthonormal set in the HH is constructed from the eigenfunction of the hypermomentum operator \mathcal{K}^2 of Eq. (13). The normalized eigenfunction with the eigenvalue $K(K+4)$ is given by

$$F_{KLM}^{\ell_1\ell_2}(\Omega_x) = \phi_K^{\ell_1\ell_2}(\alpha)[Y_{\ell_1}(\hat{\mathbf{x}}_1)Y_{\ell_2}(\hat{\mathbf{x}}_2)]_{LM}, \quad (\text{A1})$$

where K is an integer called the hypermomentum and $\phi_K^{\ell_1\ell_2}(\alpha)$ is an orthonormal function

$$\begin{aligned} \phi_K^{\ell_1\ell_2}(\alpha) \\ = \mathcal{N}_K^{\ell_1\ell_2} \cos^{\ell_1} \alpha \sin^{\ell_2} \alpha G_n(\ell_1 + \ell_2 + 2, \ell_2 + \tfrac{3}{2}; \sin^2 \alpha) \end{aligned} \quad (\text{A2})$$

with the normalization constant

$$\mathcal{N}_K^{\ell_1\ell_2} = \sqrt{\frac{2(K+2)\Gamma(\ell_1 + \ell_2 + n + 2)\Gamma(\ell_2 + n + \frac{3}{2})}{n!\Gamma(\ell_1 + n + \frac{3}{2})[\Gamma(\ell_2 + \frac{3}{2})]^2}}, \quad (\text{A3})$$

where n is an integer given by $n=(K-\ell_1-\ell_2)/2$, and G_n is the Jacobi polynomial that is expressed in terms of the Gauss hypergeometric series as follows

$$\begin{aligned} G_n(\ell_1 + \ell_2 + 2, \ell_2 + \tfrac{3}{2}; z^2) \\ = F(-n, \ell_1 + \ell_2 + n + 2, \ell_2 + \tfrac{3}{2}; z^2). \end{aligned} \quad (\text{A4})$$

Note that for $L=0$, ℓ_1 and ℓ_2 are equal and the allowed values of K are even.

One can define angles Ω_y in \mathbf{y} coordinate in completely the same way as Ω_x . The function $F_{KLM}^{\ell_1\ell_2}(\Omega_x)$, when expressed in terms of the coordinate Ω_y , becomes a linear combination of functions $F_{KLM}^{\ell'_1\ell'_2}(\Omega_y)$ with KLM being unchanged. The expansion coefficient is Raynal-Revai coefficient $\langle F_{KLM}^{\ell'_1\ell'_2}(\Omega_y) | F_{KLM}^{\ell_1\ell_2}(\Omega_x) \rangle$ [25].

Let us focus on a system of three identical particles. We want to construct a symmetric function for given K and L values by

$$F_{KLM}^\gamma = \sum_{\ell_1\ell_2} C_{\ell_1\ell_2}^\gamma F_{KLM}^{\ell_1\ell_2}(\Omega_x), \quad (\text{A5})$$

where γ is a label to distinguish different symmetric functions. The coefficient $C_{\ell_1\ell_2}^\gamma$ is determined by solving the linear equation

$$\begin{aligned} \langle F_{KLM}^{\ell_1\ell_2}(\Omega_y) | F_{KLM}^\gamma \rangle \\ = \sum_{\ell'_1\ell'_2} \langle F_{KLM}^{\ell_1\ell_2}(\Omega_y) | F_{KLM}^{\ell'_1\ell'_2}(\Omega_x) \rangle C_{\ell'_1\ell'_2}^\gamma \\ = C_{\ell_1\ell_2}^\gamma, \end{aligned} \quad (\text{A6})$$

which must be satisfied for all possible values of ℓ_1 and ℓ_2 compatible with K and L . Here the last equality is due to the fact that Ω_x in Eq. (A5) may be replaced with Ω_y because F_{KLM}^γ is a symmetric function.

We have constructed the symmetric basis functions for $L=0$. The number of symmetric functions is given by $[K/12] + 1$. When K is a multiple of 12 plus 2, however, the number is $[K/12]$. Here $[c]$ is the Gauss symbol, indicating the greatest integer that does not exceed c . We have no symmetric HH function for $K=2$.

Appendix B: Matrix element of Coulomb potential in HH basis

In this appendix we generalize the masses and charges of three particles. Let A_1, A_2, A_3 be the mass ratios $A_i = m_i/m$ of the three particles, where m is some unit mass, and Z_1e, Z_2e, Z_3e be the charges of the three particles. Let us define the coordinates \mathbf{x}_1 and \mathbf{x}_2 by

$$\begin{aligned} \mathbf{x}_1 &= \sqrt{A_{1,2}}(\mathbf{r}_1 - \mathbf{r}_2), \\ \mathbf{x}_2 &= \sqrt{A_{12,3}} \left(\frac{A_1\mathbf{r}_1 + A_2\mathbf{r}_2}{A_1 + A_2} - \mathbf{r}_3 \right), \end{aligned} \quad (\text{B1})$$

where $A_{i,j} = A_i A_j / (A_i + A_j)$, $A_{i,j,k} = (A_i + A_j) A_k / (A_i + A_j + A_k)$. In Eq. (9) m is taken to be m_α . The hyperradius ρ and hyperangle α are defined as before by $x_1 = \rho \cos \alpha$, $x_2 = \rho \sin \alpha$.

The Coulomb potential V_C acting among the particles is expressed in terms of ρ and Ω_x as follows:

$$\begin{aligned} V_C &= \frac{Z_1 Z_2 e^2}{|\mathbf{r}_1 - \mathbf{r}_2|} + \frac{Z_2 Z_3 e^2}{|\mathbf{r}_2 - \mathbf{r}_3|} + \frac{Z_3 Z_1 e^2}{|\mathbf{r}_3 - \mathbf{r}_1|} \\ &= \frac{e^2}{\rho} Q(\Omega_x) \end{aligned} \quad (\text{B2})$$

with the charge factor operator

$$\begin{aligned} Q(\Omega_x) &= \frac{Z_1 Z_2 \sqrt{A_{1,2}}}{\cos \alpha} \\ &+ \frac{Z_2 Z_3}{|\frac{\sqrt{A_{1,2}}}{A_2} \cos \alpha \hat{\mathbf{x}}_1 - \frac{1}{\sqrt{A_{12,3}}} \sin \alpha \hat{\mathbf{x}}_2|} \\ &+ \frac{Z_3 Z_1}{|\frac{\sqrt{A_{1,2}}}{A_1} \cos \alpha \hat{\mathbf{x}}_1 + \frac{1}{\sqrt{A_{12,3}}} \sin \alpha \hat{\mathbf{x}}_2|}. \end{aligned} \quad (\text{B3})$$

We calculate the matrix element of Eq. (B3) in the HH functions. The second term of $Q(\Omega_x)$ is expanded as

$$\begin{aligned} &\frac{Z_2 Z_3}{|\frac{\sqrt{A_{1,2}}}{A_2} \cos \alpha \hat{\mathbf{x}}_1 - \frac{1}{\sqrt{A_{12,3}}} \sin \alpha \hat{\mathbf{x}}_2|} \\ &= Z_2 Z_3 \sum_{\ell} \frac{s_{<\ell}}{s_{>\ell+1}} P_\ell(\cos \omega), \end{aligned} \quad (\text{B4})$$

where $s_<(s_>)$ denotes the smaller (larger) one of $\frac{\sqrt{A_{1,2}}}{A_2} \cos \alpha$ and $\frac{1}{\sqrt{A_{12,3}}} \sin \alpha$, and ω is the angle between $\hat{\mathbf{x}}_1$ and $\hat{\mathbf{x}}_2$. The matrix element of $P_\ell(\cos \omega)$ is

$$\begin{aligned} & \langle [Y_{\ell_1}(\hat{\mathbf{x}}_1)Y_{\ell_2}(\hat{\mathbf{x}}_2)]_{LM} | P_\ell(\cos \omega) | [Y_{\ell'_1}(\hat{\mathbf{x}}_1)Y_{\ell'_2}(\hat{\mathbf{x}}_2)]_{LM} \rangle \\ &= 4\pi \frac{(-1)^\ell}{2\ell+1} \sqrt{\frac{2\ell_1+1}{2\ell'_1+1}} U(\ell_1 \ell \ell'_1; \ell'_1 \ell_2) \\ & \times C(\ell \ell'_1; \ell_1) C(\ell \ell'_2; \ell_2) \end{aligned} \quad (\text{B5})$$

with

$$C(\ell_1 \ell_2; \ell_3) = \sqrt{\frac{(2\ell_1+1)(2\ell_2+1)}{4\pi(2\ell_3+1)}} \langle \ell_1 0 \ell_2 0 | \ell_3 0 \rangle, \quad (\text{B6})$$

where U is a Racah or $6j$ coefficient in a unitary form. Similarly the third term of $Q(\Omega_x)$ is expanded as

$$\begin{aligned} & \frac{Z_3 Z_1}{|\frac{\sqrt{A_{1,2}}}{A_1} \cos \alpha \hat{\mathbf{x}}_1 + \frac{1}{\sqrt{A_{12,3}}} \sin \alpha \hat{\mathbf{x}}_2|} \\ &= Z_3 Z_1 \sum_{\ell} \frac{t_{<}^\ell}{t_{>+1}^\ell} P_\ell(-\cos \omega), \end{aligned} \quad (\text{B7})$$

where $t_{<}(t_{>})$ denotes the smaller (larger) one of $\frac{\sqrt{A_{1,2}}}{A_1} \cos \alpha$ and $\frac{1}{\sqrt{A_{12,3}}} \sin \alpha$.

Combining the above results leads to the matrix element $Q_{cc'}$ ($c=(K \ell_1 \ell_2)$):

$$Q_{cc'} = \langle \phi_K^{\ell_1 \ell_2}(\alpha) | Z_L^{\ell_1 \ell_2, \ell'_1 \ell'_2}(\alpha) | \phi_K^{\ell'_1 \ell'_2}(\alpha) \rangle, \quad (\text{B8})$$

where $\langle f(\alpha) | g(\alpha) \rangle = \int_0^{\pi/2} d\alpha \cos^2 \alpha \sin^2 \alpha f(\alpha) g(\alpha)$ and

$$\begin{aligned} & Z_L^{\ell_1 \ell_2, \ell'_1 \ell'_2}(\alpha) \\ &= Z_1 Z_2 \sqrt{A_{1,2}} \delta_{\ell_1, \ell'_1} \delta_{\ell_2, \ell'_2} \frac{1}{\cos \alpha} \\ &+ \sum_{\ell} \langle [Y_{\ell_1}(\hat{\mathbf{x}}_1)Y_{\ell_2}(\hat{\mathbf{x}}_2)]_{LM} | P_\ell(\cos \omega) | [Y_{\ell'_1}(\hat{\mathbf{x}}_1)Y_{\ell'_2}(\hat{\mathbf{x}}_2)]_{LM} \rangle \\ & \times \left[Z_2 Z_3 \frac{s_{<}^\ell}{s_{>+1}^\ell} + (-1)^\ell Z_3 Z_1 \frac{t_{<}^\ell}{t_{>+1}^\ell} \right]. \end{aligned} \quad (\text{B9})$$

The range of ℓ in the above sum is limited by the triangular condition of ℓ_1, ℓ'_1, ℓ and ℓ_2, ℓ'_2, ℓ . Also both $\ell_1 + \ell'_1 + \ell$ and $\ell_2 + \ell'_2 + \ell$ must be even.

In case of three α particles, s and t are given as

$$\begin{aligned} s_{<} = t_{<} &= \begin{cases} \frac{\sqrt{3}}{2\sqrt{2}} \sin \alpha & 0 \leq \alpha \leq \frac{\pi}{6} \\ \frac{1}{2\sqrt{2}} \cos \alpha & \frac{\pi}{6} \leq \alpha \leq \frac{\pi}{2} \end{cases}, \\ s_{>} = t_{>} &= \begin{cases} \frac{1}{2\sqrt{2}} \cos \alpha & 0 \leq \alpha \leq \frac{\pi}{6} \\ \frac{\sqrt{3}}{2\sqrt{2}} \sin \alpha & \frac{\pi}{6} \leq \alpha \leq \frac{\pi}{2} \end{cases}. \end{aligned} \quad (\text{B10})$$

A more elegant way to calculate the matrix elements of the second and third terms in Eq. (B3) is to transform $\mathcal{F}_{KLM}^{\ell_1 \ell_2}$ in \mathbf{x} coordinate to those of \mathbf{y} and \mathbf{z} coordinates using the Raynal-Revai coefficients. Then we need to consider the very simple matrix element of type of the first term only.

Appendix C: Convergence of hyperspherical harmonics expansion

A three-body problem is often solved in the HH method. The accuracy of such solution depends on whether or not the HH functions with sufficiently large K values are included in the calculation. We here examine the convergence of the HH expansion. To give specific examples, we take the same wave function as Eq. (19) with a slight modification of angular momentum projection. Projecting S -waves for both \mathbf{x}_1 and \mathbf{x}_2 coordinates, we have the following shifted Gauss function

$$\begin{aligned} & \Phi_{00}(s_1, s_2, \mathbf{x}) \\ &= \mathcal{N}(s_1, s_2) \exp(-\frac{1}{2}\beta(x_1^2 + s_1^2)) i_0(\beta s_1 x_1) \\ & \times \exp(-\frac{1}{2}\beta(x_2^2 + s_2^2)) i_0(\beta s_2 x_2) [Y_0(\hat{\mathbf{x}}_1)Y_0(\hat{\mathbf{x}}_2)]_{00}, \end{aligned} \quad (\text{C1})$$

where $i_0(x) = \sinh x/x$ and $\mathcal{N}(s_1, s_2)$ is the normalization constant

$$\begin{aligned} & [\mathcal{N}(s_1, s_2)]^{-1} \\ &= \frac{\sqrt{\pi}}{4\beta^{5/2} s_1 s_2} \sqrt{(1 - \exp(-\beta s_1^2))(1 - \exp(-\beta s_2^2))}. \end{aligned} \quad (\text{C2})$$

The function (C1) has a peak at $(x_1, x_2) \sim (s_1, s_2)$, so that we obtain various configurations of 3 α particles by changing s_1, s_2 .

Expanding $\Phi_{00}(s_1, s_2, \mathbf{x})$ in the HH function as

$$\Phi_{00}(s_1, s_2, \mathbf{x}) = \sum_K f_K(s_1, s_2, \rho) F_{K00}^{00}(\Omega_x) \quad (\text{C3})$$

with

$$f_K(s_1, s_2, \rho) = \langle F_{K00}^{00}(\Omega_x) | \Phi_{00}(s_1, s_2, \mathbf{x}) \rangle, \quad (\text{C4})$$

we obtain the probability of finding K component in $\Phi_{00}(s_1, s_2, \mathbf{x})$ by a squared norm

$$\|f_K(s_1, s_2)\|^2 = \int_0^\infty d\rho \rho^5 [f_K(s_1, s_2, \rho)]^2, \quad (\text{C5})$$

which satisfies $\sum_K \|f_K(s_1, s_2)\|^2 = 1$. The distribution of $\|f_K(s_1, s_2)\|^2$ with respect to K serves as a measure of convergence of the HH expansion. Note that $\|f_K(s_1, s_2)\|^2 = \|f_K(s_2, s_1)\|^2$ for the wave function (C1).

Table III lists the values of $\|f_K(s_1, s_2)\|^2$ for some sets of $\gamma_1 = \sqrt{\beta} s_1$ and $\gamma_2 = \sqrt{\beta} s_2$ with $\beta = 4 \times 0.52 \text{ fm}^{-2}$. The rms radius, $\sqrt{\langle \rho^2 \rangle}$, calculated with the wave function is approximately given by $\sqrt{\gamma_1^2 + \gamma_2^2}/\sqrt{\beta}$. The value of $\gamma_1 = 3.5$ corresponds to the $\alpha\alpha$ distance, $\sqrt{2} s_1 = \sqrt{2/\beta} \gamma_1 \approx 3.43 \text{ fm}$, which is on the order of the $\alpha\alpha$ distance of the ${}^8\text{Be}(0^+)$ resonance. The 2α - α distance is given by $\sqrt{3/2\beta} \gamma_2$. The probability distribution quickly spreads to larger and more K values as the system size becomes larger. For $\sqrt{\gamma_1^2 + \gamma_2^2} \approx 30$, corresponding to the rms radius of 21 fm, the probability that exceeds

TABLE III: Probability in % of finding the hyperspherical harmonics with hypermomentum K in the shifted Gaussian (C1). The probability that does not exceed 0.1 % is indicated by the line –.

$\sqrt{\gamma_1^2 + \gamma_2^2}$	(γ_1, γ_2)	K															
		0	2	4	6	8	10	12	14	16	18	20	22	24	26	28	30
4.95	(3.5, 3.5)	77.7	–	20.6	–	1.6	–	–	–	–	–	–	–	–	–	–	–
21.3	(14, 16)	20.7	1.4	16.6	4.8	10.5	7.9	4.9	9.2	1.4	8.3	–	5.9	0.1	3.4	0.5	1.6
21.3	(3.5, 21)	2.2	7.7	13.7	17.3	16.9	13.0	7.5	2.8	0.3	0.2	1.6	3.2	4.0	3.7	2.7	1.6
35.0	(21, 28)	11.8	3.7	5.4	10.1	0.3	11.3	1.8	6.1	6.9	0.8	8.7	0.5	5.4	3.7	1.2	–
35.2	(3.5, 35)	0.5	1.9	4.0	6.2	8.3	9.9	10.6	10.4	9.4	7.7	5.7	3.7	2.0	0.8	0.1	–
70.1	(3.5, 70)	–	0.3	0.6	1.0	1.4	2.0	2.6	3.1	3.7	4.2	4.6	5.0	5.2	5.3	5.3	5.2
105.1	(3.5, 105)	–	–	0.2	0.3	0.5	0.6	0.8	1.1	1.3	1.6	1.8	2.1	2.3	2.6	2.8	3.0

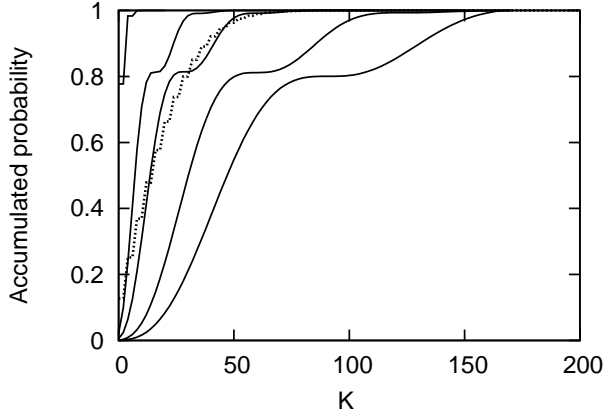


FIG. 8: Accumulated probability of finding the hyperspherical harmonics up to hypermomentum K in the shifted Gaussian (C1). Sets of (γ_1, γ_2) shown are (3.5, 3.5), (3.5, 21), (3.5, 35), (25, 25), (3.5, 70), and (3.5, 105) in increasing order of $\sqrt{\gamma_1^2 + \gamma_2^2}$. The dotted line denotes the case with (25, 25), and the solid lines the other cases.

$K = 30$ already adds up to 10%. In case where the rms radius exceeds 70 fm, the components with $K \leq 30$ are already smaller than 20%. Figure 8 displays the accumulated probability, $\sum_{K'=0}^K ||f_{K'}(s_1, s_2)||^2$, as a function of K . The plateau behavior seen in some curves is not a general feature but it is simply because γ_1 is set to 3.5. In fact the curve with $(\gamma_1, \gamma_2) = (25, 25)$ shows no plateau.

Using the specific examples we have shown that the HH convergence turns out to be slower as the system size becomes larger. This property holds true in general. Suppose that for a given wave function $\Phi(x_1, x_2)$ depending on (x_1, x_2) we want to approximate it in terms of a superposition of the HH functions. How many HH functions do we need? The values of the wave function at two points, (x_1, x_2) and (x'_1, x'_2) , on the hypersphere of a radius ρ differ when the distance of the two points is, say D , which is expressed as $D = 2\rho |\sin\{(\alpha - \alpha')/2\}| \approx \rho |\alpha - \alpha'|$, where α' is the hyperangle for (x'_1, x'_2) . Thus the number

of mesh points needed to discretize α is on the order of

$$\frac{\pi}{2} \frac{1}{|\alpha - \alpha'|} \approx \frac{\pi}{2D} \rho. \quad (\text{C6})$$

This number corresponds to the number of needed HH functions since the hypermomentum K is a quantum number related to the hyperangle α . Therefore the above result clearly shows that an increasing number of the HH functions is needed as the system or ρ increases.

Appendix D: Partial wave contents of damped plane wave

It is important to realize that the symmetrization in general brings about high partial waves between α particles. Ogata *et al.* [6] use the CDCC method in which only the S -wave continuum states of 2α particles are discretized and in addition the symmetrization is neglected. We already point out in Sec. VD that the D -wave components are necessary to account for even the long-range coupling of the Coulomb potential. An interesting question is whether or not the D -wave components can be accounted for if the symmetrized basis is used in the CDCC calculation.

To investigate this problem, we simulate the CDCC basis functions with a damped plane wave (DPW):

$$\begin{aligned} \Phi_{00}(k_1, k_2, \mathbf{x}) \\ = j_0(k_1 x_1) j_0(k_2 x_2) [Y_0(\hat{\mathbf{x}}_1) Y_0(\hat{\mathbf{x}}_2)]_{00} \exp\left(-\frac{1}{2} a \rho^2\right). \end{aligned} \quad (\text{D1})$$

Here the relative motion corresponding to the coordinate \mathbf{x}_1 or \mathbf{x}_2 is basically free S -wave but its asymptotics is made to damp using the hyperscalar Gauss function. The parameter a controls how far the DPW reaches. The wave numbers, k_1 and k_2 , are parameters that determine the density of discretized states. The symmetrized DPW is obtained by

$$\begin{aligned} \Psi_{00}(k_1, k_2) \\ = \Phi_{00}(k_1, k_2, \mathbf{x}) + \Phi_{00}(k_1, k_2, \mathbf{y}) + \Phi_{00}(k_1, k_2, \mathbf{z}). \end{aligned} \quad (\text{D2})$$

What differences do we have between the symmetrized DPW (D2) and the non-symmetrized DPW (D1) in the continuum discretization at low energies? Using a formula for the spherical Bessel function

$$j_0(\sqrt{z^2 + \zeta^2 - 2z\zeta \cos \theta}) = \sum_n (2n+1) j_n(z) j_n(\zeta) P_n(\cos \theta), \quad (\text{D3})$$

it is possible to expand the symmetrized DPW (D2) into partial waves as

$$\begin{aligned} \Psi_{00}(k_1, k_2) &= \sum_{\ell} f_{\ell}(k_1, k_2, x_1, x_2) [Y_{\ell}(\hat{\mathbf{x}}_1) Y_{\ell}(\hat{\mathbf{x}}_2)]_{00} \exp\left(-\frac{1}{2}a\rho^2\right), \end{aligned} \quad (\text{D4})$$

where ℓ is even and

$$\begin{aligned} f_{\ell}(k_1, k_2, x_1, x_2) &= \delta_{\ell,0} j_0(k_1 x_1) j_0(k_2 x_2) + \frac{1}{\sqrt{2\ell+1}} \sum_{nn'} \\ &\times ((-1)^n + (-1)^{n'}) (2n+1)(2n'+1) \langle n0n'0 | \ell 0 \rangle^2 \\ &\times j_n(\tfrac{1}{2}k_1 x_1) j_{n'}(\tfrac{\sqrt{3}}{2}k_2 x_1) j_n(\tfrac{\sqrt{3}}{2}k_1 x_2) j_{n'}(\tfrac{1}{2}k_2 x_2). \end{aligned} \quad (\text{D5})$$

The second term of the right-hand side of the above equation arises from the coordinate transformation from \mathbf{y} and \mathbf{z} to \mathbf{x} . Though Eq. (D1) contains only the S -wave, its symmetrization results in mixing higher partial waves. The quantity

$$W_{\ell} = \int_0^{\infty} dx_1 x_1^2 \int_0^{\infty} dx_2 x_2^2 \times [f_{\ell}(k_1, k_2, x_1, x_2)]^2 \exp(-ax_1^2 - ax_2^2) \quad (\text{D6})$$

gives the relative weight of ℓ -wave contained in the symmetrized DPW.

To obtain an estimate of W_{ℓ} , we choose a simple case, $k_2 = 0$. The rms radius of the DPW (D1) with $k_2 = 0$

is given by $\sqrt{\langle \mathcal{M}_{00} \rangle} = \sqrt{C(\lambda)/a}$, where $\lambda = k_1^2/a$ and $C(\lambda) = 2/3 + \lambda/[3(e^{\lambda} - 1)]$ is a monotone decreasing function bounded between $2/3 < C(\lambda) \leq 1$. The kinetic energy with Eq. (D1) is given by $[C(\lambda) + \lambda/3]\varepsilon_0$, where $\varepsilon_0 = 3\hbar^2 a/2m_{\alpha}$ is the zero-point energy confined by the radius. Thus the kinetic energy approaches $\varepsilon = (\lambda/3)\varepsilon_0 = \hbar^2 k_1^2/2m_{\alpha}$ as λ increases. Table IV lists the probability, $W_{\ell}/\sum_{\ell} W_{\ell}$, of finding the component of ℓ for some values of λ . Only for $\lambda \leq 10$, the $\alpha\alpha$ relative motion is dominated by S -wave, but otherwise the S -wave probability rapidly decreases to about 1/3. Suppose that the rms radius is of the order of $1/\sqrt{a} = 500$ fm. If ε is 0.1 MeV, k_1^2/a turns out to be about 4800 and the S -wave probability is merely 1/3. With ε of 0.01 MeV, the S -wave probability is still 40% at most. To have an S -wave dominance, ε must reduce to 0.2 keV.

The neglect of symmetrization leads to an overestimation of low-partial wave contents. It appears that symmetrizing the non-symmetrized CDCC basis functions alone does not produce the D -wave components large enough to take care of the long-range Coulomb coupling.

TABLE IV: Probability of finding the component with partial wave ℓ in the symmetrized damped plane wave (D2) with $k_2 = 0$ for several sets of k_1^2/a . Here k_1 is the wave number of the $\alpha\alpha$ relative motion and a is the falloff parameter of the hyperscalar Gauss function.

k_1^2/a	ℓ						
	0	2	4	6	8	10	≥ 12
1	1.0	0.0	0.0	0.0	0.0	0.0	0.0
10	0.907	0.092	0.001	0.0	0.0	0.0	0.0
100	0.404	0.255	0.214	0.095	0.026	0.005	0.001
1000	0.340	0.034	0.058	0.074	0.082	0.083	0.329
10000	0.334	0.004	0.006	0.009	0.012	0.014	0.621

-
- [1] F. Hoyle, *Astrophys. J. Suppl.* **1**, 121 (1954).
[2] D. N. F. Dunbar, R. E. Pixley, W. A. Wenzel, W. Whaling, *Phys. Rev.* **92**, 649 (1953).
[3] K. Nomoto, F. K. Thielemann, and S. Miyaji, *Astron. Astrophys.* **149**, 239 (1985).
[4] K. Langanke, M. Wiescher, and F.-K. Thielemann, *Z. Phys. A* **324**, 147 (1986).
[5] C. Angulo *et al.*, *Nucl. Phys. A* **656**, 3 (1999).
[6] K. Ogata, M. Kan, and M. Kamimura, *Prog. Theor. Phys.* **122**, 1055 (2009).
[7] M. Yahiro, Y. Iseri, H. Kameyama, M. Kamimura, and M. Kawai, *Prog. Theor. Phys. Suppl.* **89**, 32 (1986).
[8] A. Dotter and B. Paxton, *Astron. Astrophys.* **507**, 1617 (2009).
[9] E. Garrido, R. de Diego, D. V. Fedorov, and A. S. Jensen, *Eur. Phys. J. A* **47**, 102 (2011).
[10] N. B. Nguyen, F. M. Nunes, I. J. Thompson, and E. F. Brown, *Phys. Rev. Lett.* **109**, 141101 (2012); N. B. Nguyen, F. M. Nunes, and I. J. Thompson, *Phys. Rev. C* **87**, 054615 (2013).
[11] S. Ishikawa, *Phys. Rev. C* **87**, 055804 (2013).
[12] W. A. Fowler, G. R. Caughlan, and B. A. Zimmerman, *Annu. Rev. Astron. Astrophys.* **5**, 525 (1967).
[13] B. V. Danilin, I. J. Thompson, J. S. Vaagen, and M. V. Zhukov, *Nucl. Phys. A* **632**, 383 (1998).
[14] D. V. Fedorov and A. S. Jensen, *Phys. Lett. B* **389**, 631 (1996).
[15] S. I. Fedotov, O. I. Kartavtsev, V. I. Kochkin, and A. V. Malykh, *Phys. Rev. C* **70**, 014006 (2004).
[16] H. Matsumura and Y. Suzuki, *Nucl. Phys. A* **739**, 238

- (2004).
- [17] S. Ali and A. R. Bodmer, Nucl. Phys. **80**, 99 (1966).
 - [18] M. Chernykh, H. Feldmeier, T. Neff, P. von Neumann-Cosel, and A. Richter, Phys. Rev. Lett. **98**, 032501 (2007).
 - [19] W. J. Vermeer *et al.*, Phys. Lett. **122B**, 23 (1983).
 - [20] O. S. Kirsebom *et al.*, Phys. Rev. Lett. **108**, 202501 (2012) and references therein.
 - [21] S. Aoyama, K. Arai, Y. Suzuki, P. Descouvemont, and D. Baye, Few-Body Syst. **52**, 97 (2012).
 - [22] S. Quaglioni and P. Navrátil, Phys. Rev. Lett. **101**, 092501 (2008).
 - [23] K. Arai, S. Aoyama, Y. Suzuki, P. Descouvemont, and D. Baye, Phys. Rev. Lett. **107**, 132502 (2011).
 - [24] T. Neff, Phys. Rev. Lett. **106**, 042502 (2011).
 - [25] J. Raynal and J. Revai, Nuovo Cim. A **39**, 612 (1970).